Investigation of Electronic Structure, Optical Properties, Molecular Electrostatic Potential maps (EPM) and Aquatic toxicity of HfO2, Hf0.88Si0.12O2, Hf0.88Ge0.12O2 and Hf0.88Sn0.12O2 by computational methods

Unesco Chakma
European University of Bangladesh
Ajoy Kumer (kumarajoy.cu@gmail.com)
Bangladesh University of Engineering and Technology https://orcid.org/0000-0001-5136-6166
Tomal Hossain
European University of Bangladesh
Md. Sayed Hossain
Bangladesh Atomic Energy Commission
Md. Monsur Alam
European University of Bangladesh
Md. Shariful Islam
European University of Bangladesh
Rubel Shaikh
European University of Bangladesh
Ismat Jahan jony
European University of Bangladesh
Jahedul Islam
Presidency University

Research Article

Keywords: Band gap, DOS, Optical properties, Dielectric Function, Doping Electrostatic Potential Map (EPM), Aquatic Toxicity and DFT

Posted Date: February 15th, 2022

DOI: https://doi.org/10.21203/rs.3.rs-1260775/v1

Abstract

This research work conveys the computationally investigation of Hafnium (IV) oxide and its doped crystals by Si, Ge and Sn atom replacing on the oxygen atom in HfO_2. As Hafnium (IV) oxide has been used in power-electronics devices of MOSFETs and electronics as RRAM due to wide band gap which makes a vast problems creating high resistance. Regarding this case, the Hafnium (IV) oxide has selected and inputs how the band gap has reduced after doping the large surface area of atoms, such as Si, Ge and Sn. The lattice parameters and bandgaps were calculated with the Perdew-Burke-Ernzerhof (PBE), Revised Perdew-Burke-Ernzerhof (RPBE), Perdew Wang (PW91), Wu-Cohen (WC), and Perdew-BurkeErnzerhof for solids (PBEsol) non-local functionals of the generalized gradient approximations (GAA). The Perdew-Burke-Ernzerhof (PBE) functional provided better result which is similar to the reference value of mother crystal, HfO_2. This first principle method in view of density functional theory (DFT) focuses the structural geometry, electronic structure and optical properties employing conventional calculations pertaining to HfO_2 executing the computational tools of the CASTAP code from material studio 8.0. The band gap was recorded by 4.340 eV, 2.033 eV, 1.686 eV and 3.210 eV for HfO_2, $Hf_{0.88}Si_{0.12}O_2$ $Hf_{0.88}Ge_{0.12}O_2$ and $Hf_{0.88}Sn_{0.12}O_2$ crystals through the Generalized Gradient Approximation (GGA) with Perdew Burke Ernzerhof (PBE). Secondly, it had also justified doing further investigations by GGA with RPBE, GGA with PW91, GGA with WC and GGA with PBE_{SOL}, the band gap for HfO_2, $Hf_{0.88}Si_{0.12}O_2$, $Hf_{0.88}Ge_{0.12}O_2$ and $Hf_{0.88}Sn_{0.12}O_2$ were at 4.427 eV, 2.093 eV, 1.744 eV, and 3.262 eV, respectively using GGA with WC, 4.333 eV, 2.032 eV, 1.675 eV and 3.172 eV, respectively using GGA with PW91, 4.252 eV, 2.002 eV, 1.632eV and 3.086 eV, respectively using GGA with WC 4.245 eV, 2.001 eV, 1.629 eV, and 3.076 eV, respectively using GGA with PBE_{SOL}. Moreover the DFT and PDOS were simulated for evaluating the nature of $6s^2$, $5p^6$, $4f^{14}$, $5d^2$ orbital for a Hf atom, $3s^2$, $2p^6$ orbital for Si atom, and $4s^2$, $3p^6$, $3d^{10}$ orbital for Ge atom, $4d^{10}$, $5s^2$, $5p^2$ for Sn atom and 2s and 2p orbital for O atom of $Hf_{0.88}Ge_{0.12}O_2$ and $Hf_{0.88}Sn_{0.12}O_2$ crystals. The optical properties, for instance, absorption, reflection, refractive index, conductivity, dielectric function, loss function, electrostatic potential map and aquatic toxicity were calculated.

1.0 Introduction

In the technological era, there are many challenges raised due to development of MOSFETs for amplification the signals or voltages in current electronics devices even future generation devices having the principle of the semiconductor [1, 2]. In addition, MOSFETs consists of body, source, gate and drain, but many critical and immediate stumbling blocks are obtained during the optimization of the gate stack [3, 4]. As a result, the cardinal function of MOSFETs is not working in the proper way. Specifically, when MOSFETs is composed by HfO_2, is able to perform the much larger memory windows even no degradation of memory [5–7]. The main cause is to stay a high coercive field (1-2 MV/cm). In this case, the interfaces of HfO_2 is related with the Fermi energy level to control and amplify the electric signal or voltage from minimum conduction band (MCB) or maximum valence band (MVB) in devices, and metals body is the driving chair to operate the full procedure. Having some good user friendly properties of HfO_2, there are some drawbacks, such as crystalline life time, wide band gap, Low-frequency noise [8], γ-ray irradiation influence [9], lattice parameter [10], and gate dielectric function[11, 12]. As a result, in the principle of interface overlapping, the Si and non-Si substrates (e.g., Ge, and Sn) are added as doping to determine their opto-electronic properties developing the useable capacity in RRAM, ferromagnetic devices [2, 13], the dielectric thin films [14], band-edge CMOS applications [15].

This manuscript has organized as follows HfO_2, $Hf_{0.88}Si_{0.12}O_2$ $Hf_{0.88}Ge_{0.12}O_2$ and $Hf_{0.88}Sn_{0.12}O_2$ crystals including the electronic structure, density of states and optical properties. In this case, the GGA with PBE functional has used due to its most accuracy and acceptance for heavy metals containing crystals [16–22] with the comparing other five GGA functionals.

Doping has widely been utilized and demonstrated as an effective way to improve the performance of oxide materials. Therefore, in order to improve the uniformity of the devices, a controllable resistive mechanism of the doped-oxide should be established. In this study, the influence of Si, Ge and Sn doping on the MOSFETs, resistive random access memory (RRAM) characteristics of HfO_2-based MOSFETs and RRAM device has been illustrated. In addition, the first principle method has been performed to analyze the electronic structure, density of states and optical properties HfO_2, $Hf_{0.88}Si_{0.12}O_2$ $Hf_{0.88}Ge_{0.12}O_2$ and $Hf_{0.88}Sn_{0.12}O_2$ crystals. To calculate the comparative reflectivity, absorption and dielectric function among HfO_2, $Hf_{0.88}Si_{0.12}O_2$ $Hf_{0.88}Ge_{0.12}O_2$ and $Hf_{0.88}Sn_{0.12}O_2$, the GGA with PBE functional has used because of its accuracy [18, 23].

Finally, from the perspective of our globe, especially the 3rd world countries like Bangladesh, is going to face the 4th industrial revolution in both the industries and advance electronics material sectors, where adequate MOSFETs, resistive random access memory

(RRAM) characteristics of HfO_2-based MOSFETs and RRAM device resources and development will be necessitated, otherwise, the revolutions will be hindered due to energy and lost the achievement for the goal of next development. To solve the upcoming difficulties with advanced electronics material, the HfO_2, $Hf_{0.88}Si_{0.12}O_2$ $Hf_{0.88}Ge_{0.12}O_2$ and $Hf_{0.88}Sn_{0.12}O_2$ crystals could be one of the promising solutions in view of scientific evidence with commercial feasibilities.

2.0 Computational Methods

The first principle calculations were performed by the plane-wave basis with the pseudopotential methods in the framework of DFT, as implemented in the CASTEP code [24, 25]. We used five different non-local functionals, such as generalized gradient approximations (GGA) [26]: Perdew-Burke-Ernzerhof (PBE) [27], Revised Perdew-Burke-Ernzerhof (RPBE) [28], Perdew Wang (PW91), Wu-Cohen (WC) and Perdew-Burke-Ernzerhof for solids (PBEsol). Each exchange-correlation (XC) functional was computed using two different kinetic-energy cut-offs: 500 eV at norm conserving pseudo potentials, respectively. 2×2×2 Monkhorst-Pack grid was used. The self-consistent field (SCF) tolerance was 1.0×10^{-6}(eV/atom). The total energy tolerance, maximum ionic Hellmann-Feynman force, and maximum ionic displacement tolerance were 2.0×10^{-6} (eV/atom), 0.006 (eV/Å) and 2.0×10^{-6} (Å), respectively. For the optical spectra calculations, a dense mesh of uniformly distributed k-points is required; hence, the Brillouin zone integration was performed using a 2×4×2 grid of Monkhorst-Pack points. Next, the optical features, such as refractive index, reflectivity, absorption, conductivity and loss function, were similarly simulated for the calculation of the electronic structure and optical properties for the comparative study of band gaps for HfO_2, $Hf_{0.88}Si_{0.12}O_2$ $Hf_{0.88}Ge_{0.12}O_2$ and $Hf_{0.88}Sn_{0.12}O_2$.

3.0 Results And Discussions

3.1 Geometry of optimized structure

The lattice parameter values of HfO_2, $Hf_{0.88}Si_{0.12}O_2$, $Hf_{0.88}Ge_{0.12}O_2$ and $Hf_{0.88}Sn_{0.12}O_2$ are calculated from the materials studio after optimizing their crystal structure which is listed in the Table 1. Withal, it must be noted for optimization structure showing in figure 1(a) to 1(d) which was taken after simulation GGA with PBE, and has been considered as the standard functional of DFT having heavy metal atoms in crystal [18, 23, 29]

Table 1
Structural calculation by GGA with PBE

Crystals	a	b	c	α	β	γ	Crystal type	Space group	Density g/cm^3
HfO_2	5.040	5.074	5.269	90.00	90.00	90.00	orthorhombic	$Pca2_1$ [29]	10.37
$Hf_{0.88}Si_{0.12}O_2$	5.040	5.074	5.269	90.00	90.00	90.00	orthorhombic	$Pca2_1$ [29]	10.37
$Hf_{0.88}Ge_{0.12}O_2$	5.040	5.074	5.269	90.00	90.00	90.00	orthorhombic	$Pca2_1$ [29]	10.37
$Hf_{0.88}Sn_{0.12}O_2$	5.040	5.074	5.269	90.00	90.00	90.00	orthorhombic	$Pca2_1$ [29]	10.37

3.2 Electronic band structure

The energy difference between valence band and conduction band is known as energy/band gap (E_g). Using PBE, RPBE, PW91, WC, and PBEsol with the norm conserving pseudo potential energy/band gaps (E_g) of HfO_2, $Hf_{0.88}Si_{0.12}O_2$, $Hf_{0.88}Ge_{0.12}O_2$ and $Hf_{0.88}Sn_{0.12}O_2$ crystals were calculated. Using five functionals of DFT from CASTAP by material studio 8.0 the fermi energy level was placed at zero energy level showing in Table 2. The minimum of conduction bands (MCB) and the maximum of valence bands (MVB) for two crystals has found in G symmetry point which have been shown in Figure 2(a)–(w), which indicate indirect band gap for HfO_2. The band gap reduced after 12% Si, 12% Ge and 12% Sn atom doping on HfO_2, but the direct band gap found in case of all functionals. The crystal HfO_2 acquired indirect band gap for fear that of GGA with PBE and its value was in 4.340 eV shown in Figure 2(a) which was similar to its reference results 4.340 eV [30]. Due to have accurate result using GGA with PBE, the band gap is noticed at 2.033 eV, 1.686 eV and 3.210 eV from Figure 2(b) to 2(d) as direct band gap crystals for $Hf_{0.88}Si_{0.12}O_2$, $Hf_{0.88}Ge_{0.12}O_2$ and $Hf_{0.88}Sn_{0.12}O_2$. Moreover, for functional of GGA with RPBE, the band gap for HfO_2, $Hf_{0.88}Si_{0.12}O_2$, $Hf_{0.88}Ge_{0.12}O_2$ and $Hf_{0.88}Sn_{0.12}O_2$ is recorded at 4.427 eV, 2.093 eV, 1.744 eV and 3.262eV shown in Figure 2(e) and 2(h) also having the direct band gap crystals.

Secondly, it had also justified doing further investigations by GGA with PW91, GGA with WC, and GGA with PBEsol, the band gap for HfO_2, $Hf_{0.88}Si_{0.12}O_2$, $Hf_{0.88}Ge_{0.12}O_2$ and $Hf_{0.88}Sn_{0.12}O_2$ are at 4.333 eV, 2.032 eV, 1.675 eV and 3.172 eV, respectively using GGA with PW91, at 4.252 eV, 2.002 eV, 1.632eV and 3.086 eV, respectively using GGA with WC, and at 4.245 eV, 2.001 eV, 1.629 eV, and 3.076 eV, respectively using GGA with PBEsol shown in Figure 2(i) and 2(w).

The comparative study focused that the five GGA methods provided similar results but GGA with PBE is considered as the standard method and this method provides similar reference result at 4.340 eV for mother crystal HfO_2. The most noticeable change is found after 12% Si, 12% Ge, and 12% Sn doping in the type of band structure that the HfO_2 showed the indirect band gap which are converted in direct band gap for $Hf_{0.88}Si_{0.12}O_2$, $Hf_{0.88}Ge_{0.12}O_2$, and $Hf_{0.88}Sn_{0.12}O_2$. Furthermore, the $Hf_{0.88}Ge_{0.12}O_2$ crystal has the lowest bandgap (1.686 eV) among HfO_2, $Hf_{0.88}Si_0$.

Table 2. Band gap for HfO_2, $Hf_{0.88}Si_{0.12}O_2$ $Hf_{0.88}Ge_{0.12}O_2$ and $Hf_{0.88}Sn_{0.12}O_2$

Crystals/ functional	GGA with PBE	GGA with RPBE	GGA with PW91	GGA with WC	GGA with PBESOL	Reference
HfO_2	4.340 eV	4.427 eV	4.333 eV	4.252 eV	4.245 eV	4.340 [30]
$Hf_{0.88}Si_{0.12}O_2$	2.033 eV	2.093 eV	2.032 eV	2.002 eV	2.001 eV	Newly Predicted
$Hf_{0.88}Ge_{0.12}O_2$	1.686 eV	1.744 eV	1.675 eV	1.632 eV	1.629 eV	Newly Predicted
$Hf_{0.88}Sn_{0.12}O_2$	3.210 eV	3.262 eV	3.172 eV	3.086 eV	3.076 eV	Newly Predicted

3.3 The Density of states and Partial density of state

The density of the state indicates the point of electronic band structures and the split of an orbital. The GGA with PBE method was used to calculate the density of states (DOS) of Hf, Si, Ge, Sn and O atoms of HfO_2, $Hf_{0.88}Si_{0.12}O_2$ $Hf_{0.88}Ge_{0.12}O_2$ and $Hf_{0.88}Sn_{0.12}O_2$ crystals show in figure 3(a). Secondly, the conduction band found at the DOS of HfO_2, $Hf_{0.88}Si_{0.12}O_2$, $Hf_{0.88}Ge_{0.12}O_2$ and $Hf_{0.88}Sn_{0.12}O_2$ crystals at 0.00 eV to 5eV. The DOS of the valance band is found at -0.1 to -5 electron/eV, while the DOS of the conduction band is recorded at about 10 to 20 electron/eV. To compare the s, p, and d orbitals for both doping and undoped, the orbitals for $Hf_{0.88}Si_{0.12}O_2$ $Hf_{0.88}Ge_{0.12}O_2$ and $Hf_{0.88}Sn_{0.12}O_2$ are much higher than HfO_2, and it can be said that the Si, Ge and Sn doping on HfO_2 has increased the DOS of any crystal showing in figures 3a, 3b, 3c, 3d, and 3e.

The electronic partial density of states (PDOS) of HfO_2, $Hf_{0.88}Si_{0.12}O_2$, $Hf_{0.88}Ge_{0.12}O_2$, and $Hf_{0.88}Sn_{0.12}O_2$ crystals consist of $6s^2$, $5p^6$, $4f^{14}$, $5d^2$ orbital for a Hf atom, $3s^2$, $2p^6$ orbital for Si atom, and $4s^2$, $3p^6$, $3d^{10}$ orbital for Ge atom, $4d^{10}$, $5s^2$, $5p^2$ for Sn atom and 2s and 2p orbital for O atom, are plotted in figures 3(b) to 3(e). It can be seen that the Fermi level (E_F) is close to the maximum valence band (MVB) and the maximum conduction band (MCV). Figure 3(f) to 3(p) show that how the individual atom can contribute to create the DOS and PDOS, while the orbital of Si, Ge and Sn can significantly bestow to diminish the band gap. The p-orbital showed a high DOS close to the E_F, which become visible as a broad peak with a width of -5.0 to -1.0 eV belongs to the O-2p for HfO_2, $Hf_{0.88}Si_{0.12}O_2$, $Hf_{0.88}Ge_{0.12}O_2$, and $Hf_{0.88}Sn_{0.12}O_2$ crystals. Two peaks within range in 6–9 eV for O-2s states was observed. Regarding the Hf atoms, it has 3 clear peaks located at minor energies of about -3.0, and -2.0 eV for 4f states and 2.0 eV for 5p. Furthermore, Si atom has three significant peaks at -3.0 and 7.5 eV for 3p, another peaks at 2.5 eV for 3s. Ge atom has very small peaks at -1.5 eV, 1.0 eV, and 7.5 eV for 3d, 4s and 4p those peaks are contributed for MVB and MCB. The Sn-4d, 5p and 5s showed sharp peaks at about -1.0, 7.5, and 4.9 eV, respectively.

3.4 Optical Properties

3.4.1 Reflectivity

Reflectivity focuses on how much light is reflected from the material surface area with the amount of light incident on the material. The reflection coefficient (R) can be obtained by combining both the electric and magnetic fields of the surface for a normal event on a flat surface. In this investigation, the reflectivity of HfO_2, $Hf_{0.88}Si_{0.12}O_2$, $Hf_{0.88}Ge_{0.12}O_2$, and $Hf_{0.88}Sn_{0.12}O_2$ is shown in figure 4. The initial

reflectivity of HfO_2 has recorded 0.16 and with the increase of energy it increases. The less reflectivity means more efficient quantum dots. After doping Si%, Ge% and Sn% the initial reflectivity has recorded at 0.17, 18, and 16 which decrease with the increase of energy and proved $Hf_{0.88}Si_{0.12}O_2$, $Hf_{0.88}Ge_{0.12}O_2$, and $Hf_{0.88}Sn_{0.12}O_2$ showed the similar patterns, and the highest reflectivity is observed for Ge atom doping.

3.4.2 Absorption

The absorption coefficient provides useful data when these materials are used in solar energy conversion for optimal efficiency, and the absorption spectrum of a material depends on the nature of the energy band gap which follows the indirect band gap usually absorbs more temperature than the direct band gap semiconductor device, because there are fewer phonons at low temperature. The absorption spectrum of $Hf_{0.88}Si_{0.12}O_2$, $Hf_{0.88}Ge_{0.12}O_2$ and $Hf_{0.88}Sn_{0.12}O_2$ is higher than HfO_2. From figure 5, it is clear that with the increase of energy the absorption of materials, for instance HfO_2, $Hf_{0.88}Si_{0.12}O_2$, $Hf_{0.88}Ge_{0.12}O_2$ and $Hf_{0.88}Sn_{0.12}O_2$, is increased, but $Hf_{0.88}Ge_{0.12}O_2$ shows better value of absorption than HfO_2, $Hf_{0.88}Si_{0.12}O_2$, and $Hf_{0.88}Sn_{0.12}O_2$.

3.4.3 Refractive Index

The real part of refractive index indicates the amount of light refracted or curved and the imaginary or hypothetical part of refractive index indicates the mass loss coefficient and also determines the amount of emission when light travels through the materials. These optical properties like refractive index helps in quality evaluation of band gap persuaded structures for unremitting and optimal absorption of broad band spectral sources. Figure 6 displays the refractive index as a function of photon energy where the real part and the imaginary part for both of the HfO_2, $Hf_{0.88}Si_{0.12}O_2$, $Hf_{0.88}Ge_{0.12}O_2$ and $Hf_{0.88}Sn_{0.12}O_2$ are mentioned, showing an inverse pattern. At initial point of photon energy, the refractive index is higher for real part while the imaginary part is almost closed to 1.0 eV, and afterwards they follow a constant pattern with slightly different values of refractive index. It is same for both undoped and doped.

3.4.4 Dielectric Function

The dielectric function is most important for semiconductor device, such as diode, MOSFETs and RRAM etc. The dielectric functions are calculated in the linear optical response system within the electric dipole approximation. The necessary momentum matrix elements are obtain by using the calculated wave functions from our pragmatic pseudo potentials. Dielectric functions that describe the materials at the nanoscale are needed, opening the way to the interpretation of experimental data and design of the composites to obtain desired optical behavior [31]. The dielectric function explains how an electric field wills exertion with such an oscillating light wave element. The dielectric function is very necessary tool to investigate their optical properties which is related with adsorption properties as following equation for solid.

$$\varepsilon = \varepsilon_1(\omega) + i\varepsilon_2(\omega)$$

Here, the main part or real part of the complex dielectric function $\varepsilon_1(\omega)$ indicates the polarization and energy storage potential in the electric field of the material due to the propagated light, while the imaginary part $i\varepsilon_2(\omega)$ represents the amount of absorption in a material, and discharging of charge storage. The probability of photon absorption for the band structure of any material is closely related to the imaginary portion of the dielectric function. A significant amount of imaginary dielectric function; it represents several inter-band transitions between VB and CB. From figure 7, the real portion is always higher than the imaginary part within the energy at 1.0 eV to 1.8 eV, and it must concluded that it is the energy storage materials than discharging potential materials which helps to elaborate their applications in MOSFETs and RRAM. In case of energy range from 2 eV to 4 eV the imaginary part shows higher value than real portion for HfO_2, $Hf_{0.88}Si_{0.12}O_2$, $Hf_{0.88}Ge_{0.12}O_2$ and $Hf_{0.88}Sn_{0.12}O_2$.

3.4.5 Conductivity

A contact-free quantitative measurement sensitive to most charged reactions known as conductivity can be described in terms of band gap and electrical conduction at high (optical) frequencies[32]. Electronic conduction is nothing but putting electrons in the conduction band and by providing enough energy to an electron bound to the atoms this objective can be accomplished and can be made the electron free by breaking the bond. By shining the material with light this can easily be performed which photons do have an energy allowing the breaking of the bonds. In a solid state language, electrons can move from the valence to the conduction band by the support of photon leaving a hole in the valence band and an electrical conduction of the material will processed due to the free electron and hole. Figure 8 depicts the comparative study of the conductivity value of HfO_2, $Hf_{0.88}Si_{0.12}O_2$, $Hf_{0.88}Ge_{0.12}O_2$ and $Hf_{0.88}Sn_{0.12}O_2$ crystals. The conductivity values of both real and imaginary parts starting from almost zero at 0.0 eV. The real part of conductivity

increased with a similar trend for HfO_2, $Hf_{0.88}Si_{0.12}O_2$, $Hf_{0.88}Ge_{0.12}O_2$ and $Hf_{0.88}Sn_{0.12}O_2$ in the energy range from 0 eV to 5.0 eV and reached conductivity real peaked value 2.8 and 3.0, but the conductivity value of $Hf_{0.88}Ge_{0.12}O_2$ within energy range 1.0 to 3.0 eV is higher than HfO_2, $Hf_{0.88}Si_{0.12}O_2$, $Hf_{0.88}Ge_{0.12}O_2$ and $Hf_{0.88}Sn_{0.12}O_2$. On the other hand, the imaginary part values of HfO_2, $Hf_{0.88}Si_{0.12}O_2$, $Hf_{0.88}Ge_{0.12}O_2$ and $Hf_{0.88}Sn_{0.12}O_2$ are gradually declined after Fermi energy in the energy range from 3.0 eV and reached conductivity imaginary peaked values-2.1and -5.0.

3.4.6 Loss function

There is a number of optical parameter but energy loss function is the most significant optical parameter which is nothing but the loss of photon energy during the reaction and which is denoted by L. During passing through the element electrons losses energy and here function L describes the impetuous energy loss of electrons. The plasma resonance and the corresponding frequency which is known as plasma frequencies are very much connected with the peaks of the L function [33]. This function has capability to cover the full energy range and has involvement in scattered elastic and non-scattered electrons and also in stimulating valence inter-band transitions or electrons in the outer shell of the atom [34].

Secondly, the loss function is a crucial part of optical properties which is composed of two regions of photon energy parts such as the lower photon energy part and higher photon energy part for crystal materials. The energy loss function is closely related to the dielectric function of the photocatalyst materials within the range of the dielectric theory validation. In the energy loss function dielectric function reflects the response of a semiconductor to an external electromagnetic perturbation. The calculated exploration of loss function values for HfO_2, $Hf_{0.88}Si_{0.12}O_2$, $Hf_{0.88}Ge_{0.12}O_2$ and $Hf_{0.88}Sn_{0.12}O_2$ illustrates in figure 9. It can be seen that loss function of $Hf_{0.88}Ge_{0.12}O_2$ higher than HfO_2, $Hf_{0.88}Si_{0.12}O_2$, and $Hf_{0.88}Sn_{0.12}O_2$.

3.5 Molecular electrostatic potential maps (EPM)

The sequence of charge distribution of a molecule due to the properties of the nucleus and the nature of the electrostatic potential energy can be revealed by the electrostatic potential map which is nothing but the charge distribution of molecules in three dimensions. An area of higher than average electrostatic potential energy indicates the presence of a physically powerful positive charge or a weaker negative charger. The positive charge of the nucleus established the high potential energy value point to the absence of negative charge (less screening of the nucleus), which means that there are fewer electrons in this area. The discussion is true with low electrostatic potential which point outs an abundance of electrons. This feature of electrostatic potential can also be extrapolated to molecules. This property of electrostatic potentials can be extrapolated to molecules as well. In the figures 10 (a) to 10 (d), the positive electrostatic potential regions are highlighted in blue (electrophilic sites), where red represents the nucleophilic invasion region. Positively charged regions are observed to be significantly higher than negatively charged regions, indicating that the electrophilic groups of these molecules are more attracted to nucleophilic.

3.6 Aquatic toxicity

Aquatic toxicity is the study of the effects of chemicals and other ethnographic and natural materials and the activity on aquatic organisms that affect communities and ecosystems through individual organisms. In case of the safety of the aquatic organism, the toxicity of used materials is the crucial fact before approval to use. To create a toxicity profile for the predicted bio-inorganic crystals, computational tools through various parameters, for example AMES toxicity, honey bees, rats and fish, carcinogenicity and inhibition have been implemented. There is no response to AMES toxicity except for all crystals. Second, there is no barrier nature by all crystals by any organism, so there is no chance of entering living cells to create damage or adverse effects for other diseases, even after entering the living cell, the carcinogenic effect is almost absent. On the other hand, Table 3 Shows that the solubility of these crystals is near to organic compounds near to -3.0 or below. The innovative feedback from these crystals is explained the effect of oxygen atoms that the solubility is changed due to change in the electronegative atoms in such a way that it does not depend on electro negativity but related to size. With increasing the size, it grows up, and similar to other parameters. Finally, it could be said that these crystals are the eco-friendly materials.

Table 3
Aquatic and non aquatic toxicity

	AMES toxicity	Inhibition	Carcinogenicity	Water solubility, Log S	Acute Oral Toxicity, kg/mol	Oral Rat Acute Toxicity (LD50) (mol/kg)	Honey Bee Toxicity	Fish Toxicity pLC50 mg/L	T.Pyriformis toxicity (log µg/L)
HfO_2	No	No	No	-3.6414	0.5170	2.6333	High	1.3987 (low)	0.5238 (High)
$Hf_{0.88}Si_{0.12}O_2$	No	No	No	-3.8883	0.5163	2.6289	High	1.1513 (low)	0.6060 (High)
$Hf_{0.88}Ge_{0.12}O_2$	No	No	No	-3.7058	0.5227	2.6338	High	1.3933 (low)	0.5277 (High)
$Hf_{0.88}Sn_{0.12}O_2$	No	No	No	-3.7058	3.869	2.6338	low	1.3933 low	0.5277 (High)

4.0 Conclusion

The purpose of this work was to computationally investigate the crystal structure, electronic, and optical properties of HfO_2, $Hf_{0.88}Si_{0.12}O_2$, $Hf_{0.88}Ge_{0.12}O_2$, and $Hf_{0.88}Sn_{0.12}O_2$ using the quantum of five different correlations functionals, for example GGA with PBE, GGA with PBE, GGA with RPBE, GGA with PW91, GGA with WC, and GGA with PBE_{sol}. We ended up by using Perdew-Burke-Ernzerhof (PBE) in measuring lattice parameters, energy bandgap and optical properties of the investigated materials. The calculated energy gaps of mother crystal HfO_2 are similar to the reference value (4.340 eV). It is noticed that the 12% Si, 12% Ge and 12% Sn atom doping on HfO_2, the band gap has reduced and the $Hf_{0.88}Ge_{0.12}O_2$ crystal has a lower power band gap (1.686 eV) among HfO_2, $Hf_{0.88}Si_{0.12}O_2$, and $Hf_{0.88}Sn_{0.12}O_2$ crystals. The optical properties, due to Si, Ge and Sn doping, has changed. The optical dielectric function, absorption, reflectivity, loss function, and conductivity of $Hf_{0.88}Si_{0.12}O_2$, $Hf_{0.88}Ge_{0.12}O_2$, and $Hf_{0.88}Sn_{0.12}O_2$ are greater than HfO_2. Secondly, the molecular electrostatic potential maps (EPM), which explained the charge distribution of a molecule due to the properties of the nucleus and the nature of the electrostatic potential energy, has been calculated, and explain the factor of electronegativity for producing charge distribution. Moreover aquatic toxicity also investigated for HfO_2, $Hf_{0.88}Si_{0.12}O_2$, $Hf_{0.88}Ge_{0.12}O_2$, and $Hf_{0.88}Sn_{0.12}O_2$ crystals. Those crystals have no aquatic toxicity, such as AMES toxicity, honey bees toxicity, rats toxicity, fish toxicity, carcinogenicity toxicity, inhibition toxicity and it could be said that these crystals are the eco-friendly materials. Finally all computational results reported that Si%, Ge% and Sn% doping in HfO_2 is almost acted as a promising eco-friendly semiconductor material for MOSFETs and RRAM whereas the Ge doping is the more efficacy.

References

1. Colinge, J.-P.: Multiple-gate soi mosfets. Solid-State Electronics **48**, 897–905 (2004)
2. Lundstrom, M., Ren, Z.: Essential physics of carrier transport in nanoscale MOSFETs. IEEE Trans. Electron Devices **49**, 133–141 (2002)
3. Djeffal, F.M., M.; Benhaya: A, "A two-dimensional analytical analysis of subthreshold behavior to study the scaling capability of nanoscale graded channel gate stack DG MOSFETs". Physica E **41**, 1872–1877 (2009)
4. Swain, S.K.D., A.; Adak, S.; Pati, S.K.; Sarkar, Kumar, C.: Influence of channel length and high-K oxide thickness on subthreshold analog/RF performance of graded channel and gate stack DG-MOSFETs. Microelectron. Reliab. **61**, 24–29 (2016)
5. Cheng, C.-H., Chin, A.: Low-leakage-current DRAM-like memory using a one-transistor ferroelectric MOSFET with a Hf-based gate dielectric. IEEE electron device letters **35**, 138–140 (2013)
6. Yoon, C., Moon, S., Shin, C.: Study of a hysteresis window of FinFET and fully-depleted silicon-on-insulator (FDSOI) MOSFET with ferroelectric capacitor. Nano Convergence **7**, 1–7 (2020)
7. Richel, P.L.A., Wathelet, B., Wathelet, J.–P., Paquot, M.: "Microwave-assisted conversion of carbohydrates; State of the art and outlook.". C. R. Chim. **14**, 224–234 (2011). https://doi.org/10.1016/j.crci.2010.04.004
8. Min, B.D., S.I.V.A.P.R.A.S.A.D.; Çelik-Butler, Z.; Wang, F.; Zlotnicka, A.; Tseng, H.-H.; Tobin: Philip J, "Low-frequency noise in submicrometer MOSFETs with HfO2, HfO2/Al2O3 and HfAlOx gate stacks". IEEE Trans. Electron Devices **51**, 1679–1687 (2004)

9. Li, Y.M., Y.; Lin, W.; Dong, P.; Yang, Z.; Gong, M.; Bi, J.; Li, B.; Xi, K.; Xu: Gaobo, "Study of γ-ray irradiation influence on TiN/HfO2/Si MOS capacitor by CV and DLTS". Superlattices Microstruct. **120**, 313–318 (2018)
10. Hurley, P.K.O.C., E.; Monaghan, S.; Long, R.; O'Mahony, A.; Povey, I.M.; Cherkaoui, K.; MacHale, J.; Quinn, A.; Brammertz: Guy, "Structural and Electrical Properties of HfO_2/n-InxGa$_1$-xAs structures (x: 0, 0.15, 0.3 and 0.53)". ECS transactions **25**, 113 (2009)
11. Liu, C.C., E.F.; Tan, Seow, L.: Enhanced device performance of AlGaN/GaN HEMTs using HfO2 high-k dielectric for surface passivation and gate oxide. Semicond. Sci. Technol. **22**, 522 (2007)
12. Pradhan, D., Das, S., Dash, T., Prasanna: Study of strained-Si p-channel MOSFETs with HfO2 gate dielectric. Superlattices Microstruct. **98**, 203–207 (2016)
13. Lee, H.C., P.S.; Wu, T.Y.; Chen, Y.S.; Wang, C.C.; Tzeng, P.J.; Lin, C.H.; Chen, F.; Lien, C.H.; Tsai, M-J, "Low power and high speed bipolar switching with a thin reactive Ti buffer layer in robust HfO2 based RRAM," in *2008* IEEE International Electron Devices Meeting, 2008, pp. 1–4
14. Hsu, C.T., et al.: "High dielectric constant of RF-sputtered HfO2 thin films". Japanese journal of applied physics **31**, 2501 (1992)
15. Jagannathan, H., et al.: "Engineering high dielectric constant materials for band-edge CMOS applications". ECS transactions **16**, 19 (2008)
16. Al Mamun, A.M.A., Md; Habib, A.; Chakma, U.; Sikder, M.; Kumer, Ajoy;, "Structural, electronic, optical properties and molecular dynamics study of WO_3 $W_{0.97}Ag_{0.03}O_3$ and $W_{0.94}Ag_{0.06}O_3$ photocatalyst by the first principle of DFT study" Egyptian Journal of Chemistry, vol. 63, 2021
17. Hasan, M.M., Ajoy, K., Chakma: Unesco;, "Theoretical Investigation of Doping Effect of Fe for $SnWO_4$ in Electronic Structure and Optical Properties: DFT Based First Principle Study". Advanced Journal of Chemistry-Section A **03**, 639–644 (2020)
18. Howlader, D.H., M.S.; Chakma, U.; Kumer, A.; Islam, M.J.; Islam: Md Tawhidul; Hossain, Tomal; slam, Jahedul, "Structural geometry, electronic structure, thermo-electronic and optical properties of GaCuO2 and GaCu0. 94Fe0. 06O2: a first principle approach of three DFT functionals". Mol. Simul. **44**, 1–12 (2021). ;https://doi.org/10.1080/08927022.2021.1977295
19. ISLAM, M.T., Ajoy, K.U.M.E.R., HOWLADER, Debashis; CHAKMA, Kamal Bikash, C.H.A.K.M.A.: Unesco;, "Electronics structure and optical properties of $Mg(BiO_2)_4$ and $Mg(Bi_{0.91}Ge_{0.083}O_2)_4$: A first principle approach". Turkish Computational and Theoretical Chemistry **4**, 24–31 (2020)
20. B.C. Kamal,;Ajoy, K.; Unesco, C.; Debashis, H.; Md Tawhidul, Islam;, "A theoretical investigation for electronics structure of $Mg(BiO_2)_2$ semiconductor using first principle approach," *International Journal of New Chemistry*, vol. 7, pp. 247-255., 2020
21. Mokit, S.U.M.A.: Chakma,; Ajoy Kumer,; Mohammad,Jahidul Islam, Ahsan Habib; Md Monsur Alam;, "The Exploration of Structural, Electronic and Optical Properties for MoS_2 and $Mo_{0.95}W_{0.05}S_2$ Photocatalyst Effort on Wastewater Treatment using DFT Functional of First Principle Approach". Applied Journal of Environmental Engineering Science **7**, 103–113 (2021)
22. C.D. Md Tawhidul Islam; Ajoy Kumer; Unesco, Howlader;, "A Computational Investigation of Electronic Structure and Optical Properties of $AlCuO_2$ and $AlCu_{0.96}Fe_{0.04}O_2$: A First Principle Approach," *Orbital: Electron. J. Chem*, vol. 13, 2021
23. Ali, M.I., M.J.; Rafid, M.; Ahmed, R.; Jeetu, Md; Rayhan, R.; Roy, R.; Chakma, U.; Kumer: Ajoy, "The computational screening of structural, electronic, and optical properties for SiC, $Si_{0.94}Sn_{0.06}C$, and $Si_{0.88}Sn_{0.12}C$ lead-free photovoltaic inverters using DFT functional of first principle approach". Eurasian Chemical Communications **3**, 327–338 (2021)
24. Segall, M., D.; Lindan, P.J.D.; Probert, M.Jal; Pickard, C.J.; Hasnip, P.J.; Clark, S.J.; Payne: M., C.,, "First-principles simulation: ideas, illustrations and the CASTEP code". J. Phys.: Condens. Matter. **14**, 2717 (2002)
25. Clark, S.J.S., M.D.; Pickard, C.J.; Hasnip, P.J.; Probert, M.I.J.; Refson, K.; Payne, Mike, C.: First principles methods using CASTEP. Zeitschrift für Kristallographie-Crystalline Materials **220**, 567–570 (2005)
26. Ziesche, P.K., S.; Perdew: John P;, "Density functionals from LDA to GGA". Comput. Mater. Sci. **11**, 122–127 (1998)
27. del Campo, J.M.G., J.L.; Trickey, S.B.; Vela, Alberto, "Non-empirical improvement of PBE and its hybrid PBE0 for general description of molecular properties," *The Journal of chemical physics*, vol. 136, p. 104108, 2012
28. Yang, Z.J., Zhao, K., Truhlar, Y.: DG, "Tests of the RPBE, revPBE, tau-HCTHhyb, omegaB97X-D, and MOHLYP density functional approximations and 29 others against representative databases for diverse bond energies and barrier heights in catalysis". J. Chem. Phys. **132**, 164117 (2010)
29. Ajoy, K., Chakma, U., "Developing the amazing photocatalyst of $ZnAg_2GeSe_4$, $ZnAg_2Ge_{0.93}Fe_{0.07}Se_4$ and $ZnAg_2Ge_{0.8}6Fe_{0.14}Se_4$ through the computational explorations by four DFT functionals," *Heliyon*, vol. 7, p. e07467, 2021

30. Zhu, H., et al.: "Recent progress in ab initio simulations of hafnia-based gate stacks". Journal of Materials Science **47**, 7399–7416 (2012)
31. Alves-Santos, M., et al.: "Dielectric functions of semiconductor nanoparticles from the optical absorption spectrum: the case of CdSe and CdS". J. Phys. Chem. C **114**, 3776–3780 (2010)
32. Eichelbaum, M.S.e., R.; Karpov, A.; Dobner, C.-K.; Rosowski, F.; Trunschke, A.; Schlögl: Robert, "The microwave cavity perturbation technique for contact-free and in situ electrical conductivity measurements in catalysis and materials science". Physical Chemistry Chemical Physics **14**, 1302–1312 (2012)
33. Treumann, R.A.: The electron–cyclotron maser for astrophysical application. Astron. Astrophys. Rev. **13**, 229–315 (2006)
34. Livache, C.G., N.; Gréboval, C.; Martinez, B.; Ramade, J.; Qu, J.; Triboulin, A.; Cruguel, H.; Baptiste, B.; Klotz: Stefan, "Effect of Pressure on Interband and Intraband Transition of Mercury Chalcogenide Quantum Dots". J. Phys. Chem. C **123**, 13122–13130 (2019)

Figures

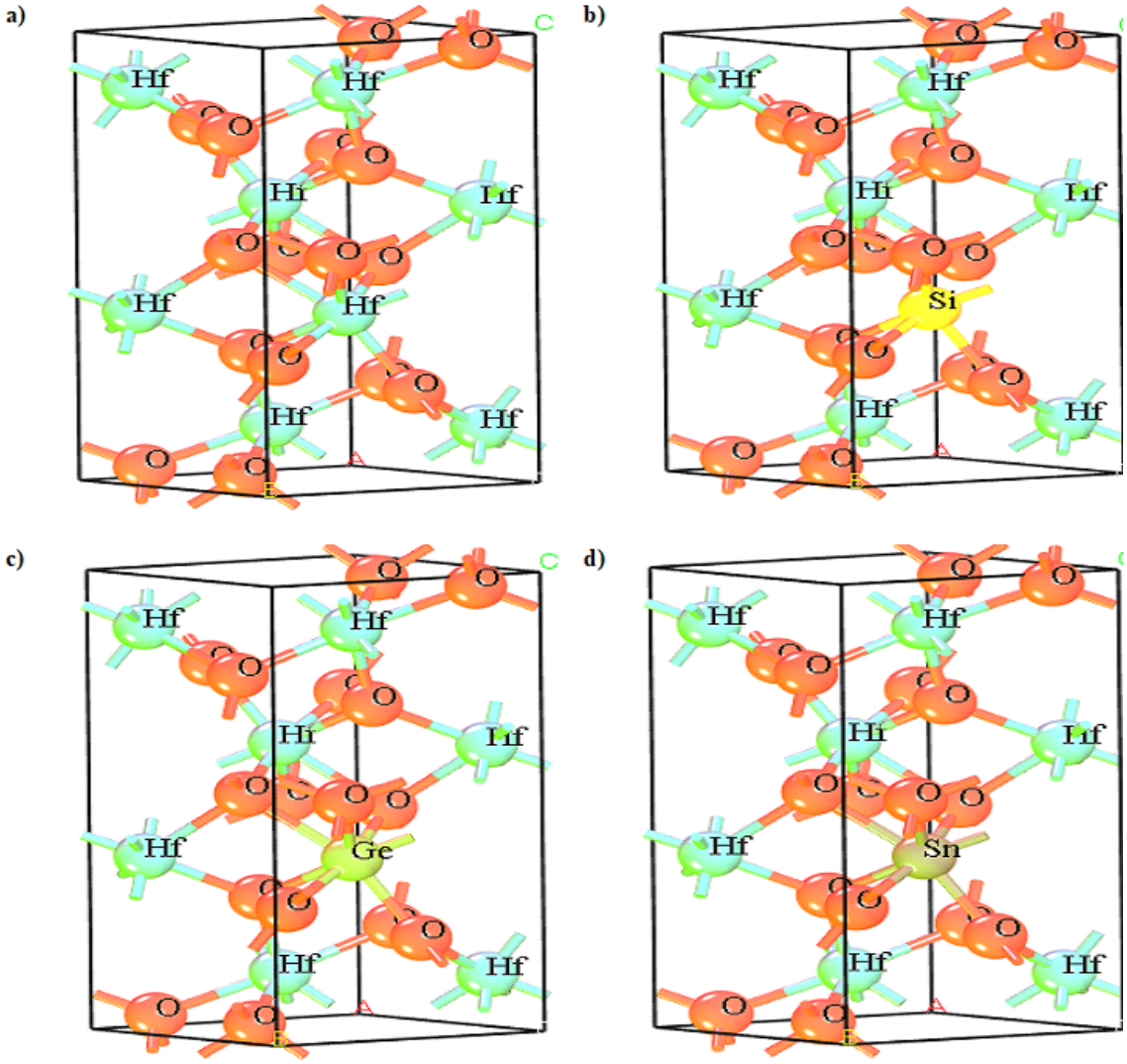

Figure 1

a) Structure for HfO_2, b) Structure for $Hf_{0.88}Si_{0.12}O_2$, c) Structure for $Hf_{0.88}Ge_{0.12}O_2$ and d) Structure for $Hf_{0.88}Sn_{0.12}O_2$.

Figure 2

a) Band structure by GGA with PBE for HfO_4, b) Band structure by GGA with PBE for $Hf_{0.88}Si_{0.12}O_4$, c) Band structure by GGA with PBE $Hf_{0.88}Ge_{0.12}O_4$, d) Band structure by GGA with PBE for $Hf_{0.88}Sn_{0.12}O_4$, e) Band structure by GGA with RPBE for HfO_4, f) Band structure by GGA with RPBE for $Hf_{0.88}Si_{0.12}O_4$, g) Band structure by GGA with RPBE for $Hf_{0.88}Ge_{0.12}O_4$, h) Band structure by GGA with RPBE for $Hf_{0.88}Sn_{0.12}O_4$, i) Band structure by GGA with PW91for HfO_4, j) Band structure by GGA with PW91 for $Hf_{0.88}Si_{0.12}O_4$, k) Band structure GGA with PW91 $Hf_{0.88}Ge_{0.12}O_4$, l) Band structure by GGA with PW91for $Hf_{0.88}Sn_{0.12}O_4$, m) Band structure by GGA with WC for HfO_4, n) Band structure by GGA with WC for $Hf_{0.88}Si_{0.12}O_4$, o) Band structure by GGA with WC for $Hf_{0.88}Ge_{0.12}O_4$, p) Band structure by GGA with WC for $Hf_{0.88}Sn_{0.12}O_4$, q) Band structure by GGA with PBESOL for HfO_4, s) Band structure by GGA with PBESOL for $Hf_{0.88}Si_{0.12}O_4$, t) Band structure by GGA with PBESOL for $Hf_{0.88}Ge_{0.12}O_4$ and w) Band structure by GGA with PBESOL for $Hf_{0.88}Sn_{0.12}O_4$.

Figure 3

a) Total density of states for HfO_2, $Hf_{0.88}Si_{0.12}O_2$ $Hf_{0.88}Ge_{0.12}O_2$ and $Hf_{0.88}Sn_{0.12}O_2$, b) Partial density of states for HfO_2, c) Partial density of states for $Hf_{0.88}Si_{0.12}O_2$, d) Partial density of states for $Hf_{0.88}Ge_{0.12}O_2$, e) Partial density of states for $Hf_{0.88}Sn_{0.12}O_2$, f) Hf atom for HfO_2, h) Hf atom for $Hf_{0.88}Si_{0.12}O_2$, i) Si atom for $Hf_{0.88}Si_{0.12}O_2$, j) O atom for $Hf_{0.88}Si_{0.12}O_2$, k) Hf atom for $Hf_{0.88}Ge_{0.12}O_2$, l) Ge atom for $Hf_{0.88}Ge_{0.12}O_2$, m) O atom for $Hf_{0.88}Ge_{0.12}O_2$, n) Hf atom for $Hf_{0.88}Sn_{0.12}O_2$, O) Sn atom for $Hf_{0.88}Sn_{0.12}O_2$, p) O atom for $Hf_{0.88}Sn_{0.12}O_2$.

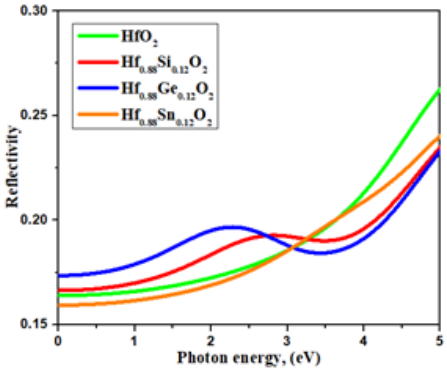

Figure 4

Reflectivity

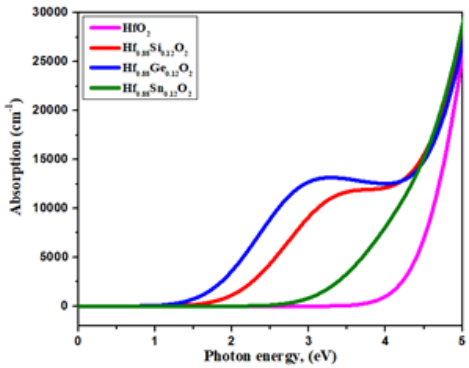

Figure 5

Absorption

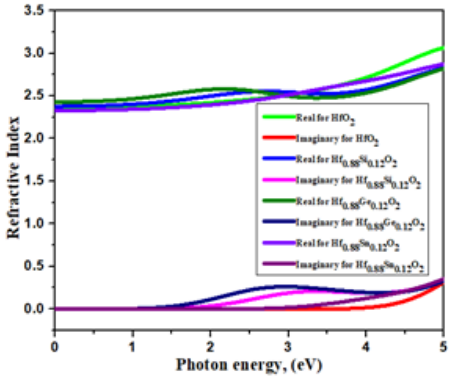

Figure 6

Refractive Index

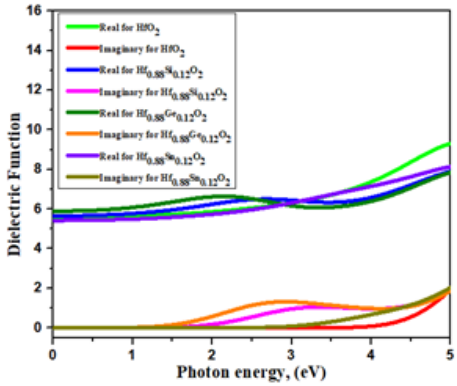

Figure 7

Dielectric Function

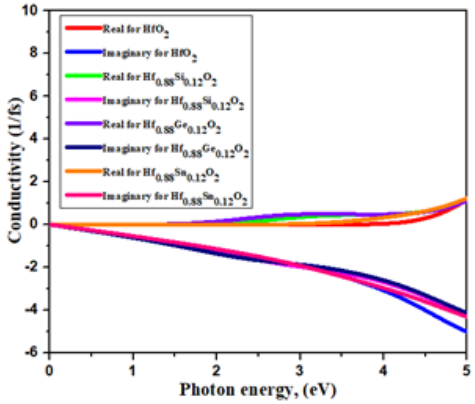

Figure 8

Conductivity

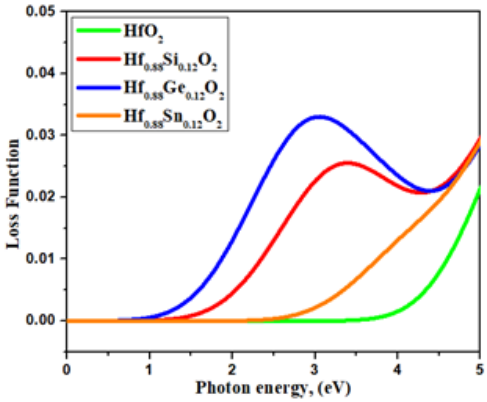

Figure 9

Loss Function

Figure 10

a) Molecular electrostatic potential map for HfO_2, b) Molecular electrostatic potential map for $Hf_{0.88}Si_{0.12}O_2$, c) Molecular electrostatic potential map for $Hf_{0.88}Ge_{0.12}O_2$, and d) Molecular electrostatic potential map for $Hf_{0.88}Sn_{0.12}O_2$.

Supplementary Files

This is a list of supplementary files associated with this preprint. Click to download.

- floatimage1.jpeg